

PINIP based high-speed high-extinction ratio micron-size silicon electro-optic modulator

Sasikanth Manipatruni, Qianfan Xu, Michal Lipson

School of Electrical and Computer Engineering, Cornell University, Ithaca, N.Y. 14850
lipson@ece.cornell.edu

Abstract: We propose an electro-optic device in silicon based on a p-i-n-i-p device structure for charge transport. The proposed device exhibits carrier injection time of 10 ps and extraction time of 15 ps enabling 100 GHz operation. When integrated into a resonator the micron-size device operates at 40 Gbit/s with 12 dB extinction ratio and 2.25 fJ/bit/micron-length power dissipation. The proposed device is limited in speed only by the photon lifetime of the resonator.

©2007 Optical Society of America

OCIS codes: (130.3130) Integrated optical materials; (130.3120) Integrated optical devices; Ring resonators(230.5750)

References

1. L. C. Kimerling, D. Ahn, A. B. Apsel, M. Beals, D. Carothers, Y-K. Chen, T. Conway, D. M. Gill, M. Grove, C-Y Hong, M. Lipson, J. Liu, J. Michel, D. Pan, S. S. Patel, A. T. Pomerene, M. Rasras, D. K. Sparacin, K-Y. Tu, A. E. White, and C. W. Wong, "Electronic-photonics integrated circuits on the CMOS platform," *Proc. SPIE* **6125**, 612502 (2006).
2. A. Liu, R. Jones, L. Liao, D. Samara-Rubio, D. Rubin, O. Cohen, R. Nicolaescu, and M. Paniccia, "A high-speed silicon optical modulator based on a metal-oxide-semiconductor capacitor," *Nature* **427**, 615-618 (2004).
3. Q. Xu, B. Schmidt, S. Pradhan, and M. Lipson, "Micrometre-scale silicon electro-optic modulator," *Nature* **435**, 325-327, (2005)
4. L. Zhou and A. W. Poon, "Silicon electro-optic modulators using p-i-n diodes embedded 10-micron-diameter microdisk resonators," *Opt. Express* **14**, 6851-6857 (2006)
5. B. Schmidt, Q. Xu, J. Shakya, S. Manipatruni, and M. Lipson, "Compact electro-optic modulator on silicon-on-insulator substrates using cavities with ultra-small modal volumes," *Opt. Express* **15**, 3140-3148 (2007)
6. F. Gan and F. X. Kärtner, "High-Speed Electrical Modulator in High-Index-Contrast (HIC) Si-Waveguides," in *Conference on Lasers and Electro-Optics, Technical Digest (CD)* (Optical Society of America, 2007), CMG1.
7. G. Gunn, "CMOS photonics™ - SOI learns a new trick," in *Proceedings of IEEE International SOI Conference Institute of Electrical and Electronics Engineers, New York*, (2005), 7-13.
8. A. Liu, L. Liao, D. Rubin, H. Nguyen, B. Ciftcioglu, Y. Chetrit, N. Izhaky, and M. Paniccia, "High-speed optical modulation based on carrier depletion in a silicon waveguide," *Opt. Express* **15**, 660-668 (2007)
9. R. Soref, B. Bennett, "Electrooptical effects in silicon," *IEEE J. Quantum Electron.*, **23**, no.1. 123- 129, (1987)
10. H. W. Lutz, , a, A. Schwanhäuber, M. Eckardt, L. Robledob, G. Döhlerb and A. Seilmeier, "High-field electron transport in GaAs/AlxGa1-xAs p-i-n-i-p-structures investigated by ultrafast absorption changes", *Physica E: Low-dimensional Systems and Nanostructures* **13**, Issues 2-4, (2002), 802-805
11. SILVACO International, 4701 Patrick Henry Drive, Bldg. 1, Santa Clara, CA 94054.
12. C.A. Barrios, V.R. Almeida, R. Panepucci, M. Lipson, "Electrooptic modulation of silicon-on-insulator submicrometer size waveguide devices", *J. Lightwave Technol.* **21**, 2332 – 2339 (2003).
13. P. D. Hewitt and G. T. Reed, "Improved modulation performance of a silicon p-i-n device by trench isolation," *J. Lightwave Technol.* **19**, 387 (2001).
14. B. Jalali, O. Boyraz, D. Dimitropoulos, V. Raghunathan, "Scaling laws of nonlinear silicon nanophotonics" *Proceedings of SPIE*, **5730**, 41-51 (2005)
15. H. C. Huang, S. Yee, and M. Soma, "Quantum calculations of the change of refractive index due to free carriers in silicon with nonparabolic band structure," *J. Appl. Phys.* **67**, 2033-2039 (1990).
16. T. Kuwayama, M. Ichimura, E. Arai, "Interface recombination velocity of silicon-on-insulator wafers measured by microwave reflectance photoconductivity decay method with electric field," *Appl. Phys. Lett.* **83**, 928-930, (2003)
17. Palais, A. Arcari, "Contactless measurement of bulk lifetime and surface recombination velocity in silicon wafers," *J. Appl. Phys.* **93**, 4686-4690, (2003)
18. Pierret, R. F. *Advanced Semiconductor Fundamentals*. 1987 Addison-Wesley Longman Publishing Co., Inc.

19. V. R. Almeida, C. A. Barrios, R. R. Panepucci, and M. Lipson, *Nature* **431**, 1081 (2004).
20. A. Yariv, "Universal relations for coupling of optical power between micro resonators and dielectric waveguides," *Electron. Lett.* **36**, 4 (2000)
21. Q. Xu, S. Manipatruni, B. Schmidt, J. Shakya, and M. Lipson, "12.5 Gbit/s carrier-injection-based silicon micro-ring silicon modulators," *Opt. Express* **15**, 430-436 (2007)
22. Bedair, S.M.; McDermott, B.T.; Reid, K.G.; Neudeck, P.G.; Cooper, J.A., Jr.; Melloch, M.R., "Extremely low-leakage GaAs P-i-N junctions and memory capacitors grown by atomic layer epitaxy," *Electron Device Letters IEEE* **11**, 261 – 263 (1990).
23. Yamada, K.; Nakamura, K.; Horikawa, H. , "Electroabsorption modulator with PINIP structure", *Electron. Lett.*, **34**, 304-306 (1998).
24. Q. Xu, B. Schmidt, J. Shakya, and M. Lipson, "Cascaded silicon micro-ring modulators for WDM optical interconnection," *Opt. Express* **14**, 9431-9435 (2006)
25. L. Liao, D. Samara-Rubio, M. Morse, A. Liu, D. Hodge, D. Rubin, U. Keil, and T. Franck, "High speed silicon Mach-Zehnder modulator," *Opt. Express* **13**, 3129-3135 (2005)
26. Little, B.E.; Chu, S.T.; Haus, H.A.; Foresi, J.; Laine, J.-P. , "Microring resonator channel dropping filters", *J. Lightwave Technol.* **15**, 998-1005 (1997).
27. Emelett, S. & Soref, R. Analysis of dual-microring-resonator cross-connect switches and modulators. *Opt. Express* **13**, 7840–7853 (2005).
28. Little, B.E.; Foresi, J.S.; Steinmeyer, G.; Thoen, E.R.; Chu, S.T.; Haus, H.A.; Ippen, E.P.; Kimerling, L.C.; Greene, W. , "Ultra-compact Si-SiO₂ microring resonator optical channel dropping filters", *IEEE Photon. Technol. Lett. IEEE*, **10**, 549-551 (1998).
29. T.K. Woodward; A.V. Krishnamoorthy; K.W. Goossen; J.A. Walker; B. Tseng; J. Lothian; S. Hui; R. Leibenguth, "Modulator-driver circuits for optoelectronic VLSI", *IEEE Photon. Technol. Lett.* **9**, 839 – 841 (1997).

1. Introduction

An all-silicon electro-optic modulator is a key component in electronic photonic integrated circuits [1]. Carrier-dispersion-based electro-optic modulators on silicon-on-insulator (SOI) substrates have been demonstrated based on a MOS capacitor [2], a PIN diode [3-6] or a PN junction [7, 8]. However in order to achieve devices with high extinction ratio for large data rates on a small silicon footprint, one needs to break the traditional tradeoff between speed and extinction ratio. MOS-based devices can potentially scale in speed to many tens of Gbits/s, however the effective index change obtained is limited due to the small overlap of the optical mode with carrier concentration change. On the other hand, PIN-based devices with laterally-formed junctions provide high extinction ratio but are limited in speed due to the carrier injection dynamics. Hence a tradeoff exists between speed and extinction ratio due to the available electro-optic structures. Here, we propose a device which achieves both high speed and high extinction ratio through a novel doping profile. The proposed device consists of two back-to-back diodes formed by laterally doped layers of p-i-n-i-p. The electrical rise and fall times are 10 ps and 15 ps respectively which approach the fundamental limit imposed by carrier terminal velocity in silicon for waveguide geometries dictated by index contrast in SOI substrates. Based on such a structure we propose an electro-optic modulator that operates at 40 Gbit/s non-return to zero (NRZ) with a high extinction ratio (>10 dB) within the dimensions of ~10 microns.

2. Device description

The proposed device consists of a waveguide embedded in a PINIP device (see Fig. 1). The PINIP device provides high speed transitions of carrier density in the waveguide. The refractive index of the waveguide is modulated due to the carrier dispersion effect in silicon [9]. The doping levels and dimensions of the device are outlined in Table 1. The device cross section is shown in Figure 1.

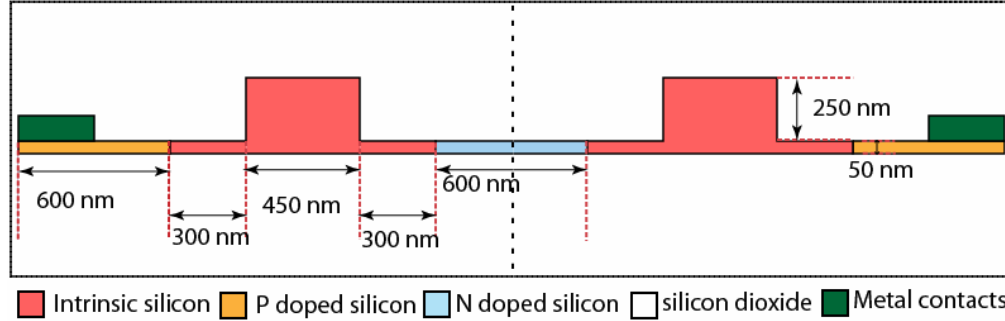


Fig. 1. Proposed PINIP device; the device is symmetric about the central dotted line.

Table 1. PINIP Device Parameters

Intrinsic region doping	$5 \times 10^{16}/\text{cm}^3$
N region doping	$10^{19}/\text{cm}^3$
P region doping	$10^{19}/\text{cm}^3$
N region width	600 nm
Waveguide dimensions (width x height)	450 nm x 250 nm
Distance from waveguide edge to doped regions	300 nm

The proposed PINIP device operates as a high field transport device where carriers are accelerated through the intrinsic region at the saturation velocity in silicon. This structure has been traditionally used for study of high field behavior of electrons (NIPIN) and holes (PINIP) [10]. Here we propose to use the high field, near saturation velocity transport in PINIP for electro-optic modulation in an SOI photonic device. One of the two ridges shown in Fig. 1 is used for guiding light; the other ridge is used as a charge reciprocating structure. The double ridge structure creates symmetry in the electrical response of the PINIP device. The charge injecting regions are connected to the strip waveguide through a 50 nm thick slab of intrinsic silicon. The entire structure is clad in SiO_2 . The charge injecting regions have uniform doping concentrations of $10^{19}/\text{cm}^3$. The wave guiding regions are slightly p doped with a typical dopant concentration of $5 \times 10^{16}/\text{cm}^3$ so that the carrier density changes are unipolar. This significantly decouples the performance of the device from the time response of recombination of electrons and holes. This is important in order to avoid pattern dependency and timing jitter associated with carrier dispersion devices due to recombination effects.

3. Modeling

The electrical modeling was carried out in SILVACO device simulation software [11]. The software models the internal physics of the device by numerically solving the Poisson and charge continuity equations. The suitability of SILVACO for simulation of these characteristics has been established by prior works [12-14]. We included Shockley Read Hall (SRH), Auger and direct recombination models. We outline the models and parameters used in Table 2.

The free carrier dispersion of silicon is modeled by the following equations for the refractive index and absorption coefficient for a wavelength of $1.55 \mu\text{m}$ in silicon [9].

$$\Delta n = \Delta n_e + \Delta n_h = -(8.8 \times 10^{-22} \Delta n + 8.5 \times 10^{-18} (\Delta p)^{0.8})$$

$$\Delta \alpha = \Delta \alpha_e + \Delta \alpha_h = 8.5 \times 10^{-18} \Delta n + 6.0 \times 10^{-18} \Delta p$$

where Δn is the change in refractive index, $\Delta \alpha$ is the change in absorption coefficient of intensity, ΔN is the injected electron density per cm^3 , and ΔP is the injected hole density per

cm³. The deviation from the classical Drude model is included in the 0.8 power dependency on the hole concentration which arises due to the non-parabolic shape of the band structure of silicon [15].

Table 2. Main parameters used in electrical modeling

Bulk silicon electron lifetime (μs)	3 [12]
Bulk silicon hole lifetime (μs)	10 [12]
Carrier interface recombination velocity (cm/s)	10^4 (un-passivated), 100 (passivated) [14, 16, 17]
Carrier surface recombination velocity (cm/s)	10^4 (un-passivated), 100 (passivated) [14, 16, 17]
Interface trap density ($\text{cm}^{-2} \text{eV}^{-1}$)	10^{10} [18]

4. Operating principle and electrical response of the PINIP device

The proposed PINIP device consists of two adjacent diodes in opposite directions. The charge transport takes place only during the turn-on and turn-off times of the diodes resulting in fast carrier density changes. The turn-on and turn-off times of the diodes are determined by the time taken for the carriers to form the depletion region as they are swept under high electric fields. The carriers are accelerated to the carrier terminal velocity in silicon (10^7 cm/s) under electric fields exceeding 10^4 V/cm. By using a symmetric electrical structure for the diodes we produce fast transients during the build up of and depletion of carriers.

We simulated the transient electrical and optical characteristics of the device. The electrical transient characteristics show that the PINIP device conducts only during the transition time of the applied voltage thus creating fast electrical transitions. In Fig. 2 (a) we show the carrier density at the center of the waveguide for an applied voltage of ± 3 V with 10 ps rise and 15 ps fall times. In Fig. 2 (b) we show the anode current per micron length of the device. The asymmetry in the rise and fall times is due to the non-uniform distribution of the electric field in the intrinsic region. The rise time is determined by the transit time of carriers from the thin slab region to the center of the waveguide region. The electric field in the slab region is higher than the electric field in the waveguide region, leading to a faster rise time (10 ps) as compared to the fall time.

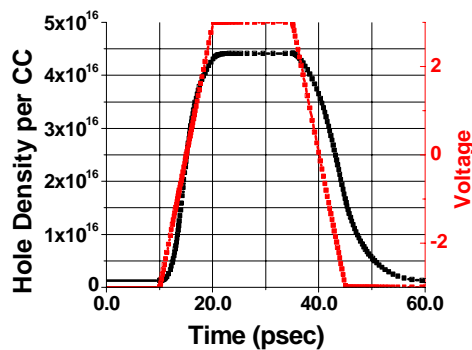


Fig. 2(a) Carrier Density in the center of the ridge

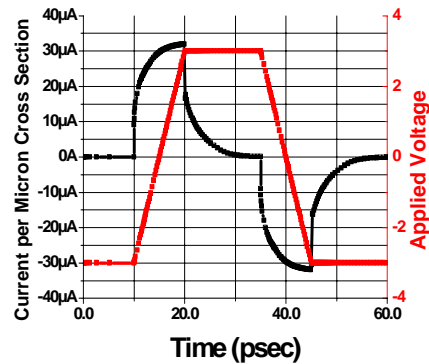


Fig. 2(b) Anode Current

The rise time of this device is 2 orders of magnitude smaller than the rise time in PIN carrier injection devices which is on the order of 1 ns (determined by the free carrier lifetime [19]). The device also shows reduced dependence of peak carrier density on the applied

voltage. This reduces the effect of noise in the applied voltage on the output waveforms. In Fig. 3 (a), we show the dependence of peak charge injection on applied voltage. This is in contrast with PIN-based devices where the ON state charge density is exponentially related to applied voltage due to which the noise in ON state is directly seen in ON state optical transmission. In Fig. 3 (b), we show the variation in charge dynamics as the intrinsic region doping is varied from $5 \times 10^{16} \text{ cm}^{-3}$ to $8 \times 10^{16} \text{ cm}^{-3}$. The dual-diode PINIP device provides a way to control the injected charge while enabling high speed transitions. When a positive voltage is applied, the injection of carriers stops as soon as the second diode goes into reverse bias. As a consequence, the injected charge is limited to the charge required to reverse-bias the second diode. Hence we see that the injected charge is clamped to the intrinsic hole concentration (which is identical in both diodes). Similarly, when a negative voltage is applied, the first PIN region will be reverse-biased and the charge injected into the second PIN region is controlled by the first PIN region. From figure 3 (b), one can see clearly that the peak charge concentration is controlled by the amount of charge that can be exchanged between the forward and reverse diodes.

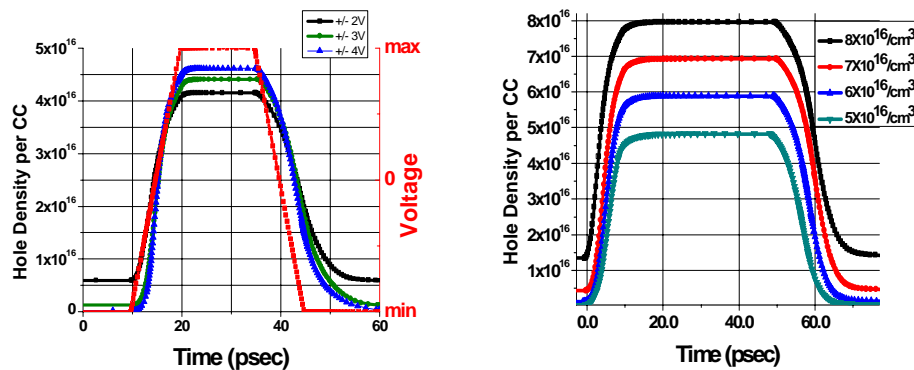


Fig. 3. Charge transients in the center of the waveguide in the PINIP device with a) applied voltages of 2 V, 3 V and 4 V b) varied intrinsic region doping concentration (electron density is negligible since the intrinsic region is lightly p doped)

5. Optical structure

As an example of a possible electro-optic modulator device based on the above electrical structure we propose a device based on a ring resonator as shown in Fig. 4. The electro-optic modulator is formed by integrating a PINIP structure around a silicon ring cavity on an SOI platform.

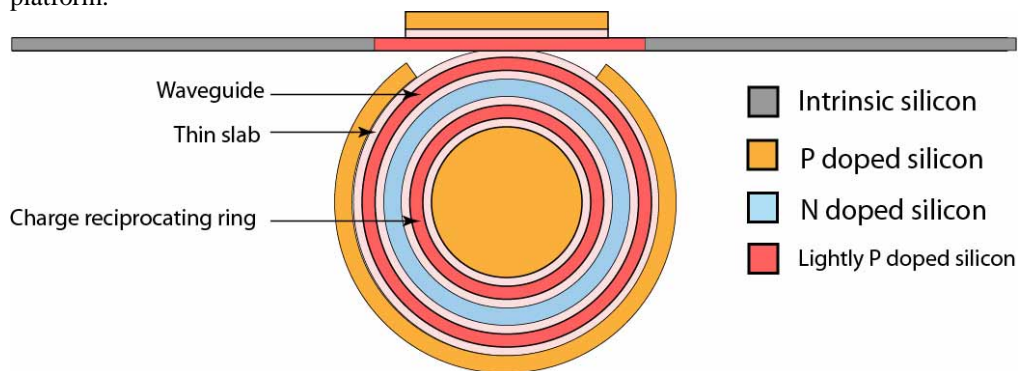


Fig. 4. A ring resonator integrated into a PINIP structure

Note that only the outer ring supports an optical mode while the inner ring is used only as part of the electrical PINIP structure. (See Fig. 1).

We analyze the transient optical response of the PINIP double-ridge ring modulator and compare it with the optical response of a PIN embedded ring modulator. Both the devices were assumed to be fabricated using waveguides with a 1 ns carrier life time [19] (total surface recombination velocity of 16,000 cm/s due to surface recombination and interface recombination). We modeled the ring resonator as a ring cavity with a lossless coupler as an input [20]. The ring cavity is simulated by iteratively calculating the fields in the ring and the coupler. Figure 6, shows the response to a symmetric square pulse of ± 2.5 V for modulators with a quality factor of 20,000. In the PIN modulator one can observe the effect of storage time due to accumulated carriers, while in the PINIP modulator this effect is not present. A chirp-like transient at the rising edge of optical transmission is apparent in Fig. 5. This transient improves the eye opening as seen in [21] and is caused by the interference between optical energy being released from the cavity and the input optical energy [21]. The optical fall time of the PINIP modulator is given by the photon lifetime of the cavity. The turn-off time is determined by the optical ring-down time of the cavity given by the photon lifetime ($\lambda^2/2\pi c\Delta\lambda=16$ ps) for a cavity with a quality factor of 20,000).

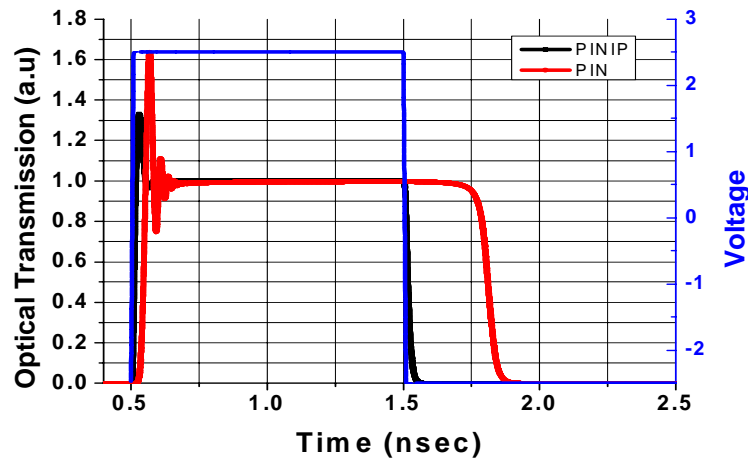


Fig. 5. The optical transient response of the PINIP embedded ring modulator compared to a PIN-embedded ring modulator.

6. Decoupling the device performance from the carrier lifetime

Since the device is unipolar, the effect of the carrier recombination on the device performance is small in the absence of the oppositely charged carriers. Note that even though the surface states at the oxide/silicon interface act as traps for the carriers they do not lead to recombination. This is in strong contrast to PIN-based device performance which strongly depends on the recombination lifetime. In Fig. 6, we show the transmission of both PIN and PINIP devices for surface recombination velocities (SRVs) of 100 cm/s to 20,000 cm/s. One can clearly see the strong performance dependence of the PIN device on the SRV in strong contrast to the performance of PINIP devices which shows no SRV dependence.

The PINIP devices can modulate data with extremely long identical bit sequences since the state hold time is >1 μ s in the absence of carrier recombination processes. The state hold time is limited by the leakage current of the structure [22] which mainly arises from thermal generation in the depletion region. The PINIP devices also do not suffer from the timing jitter that is characteristic of PIN-based carrier injection modulators [23].

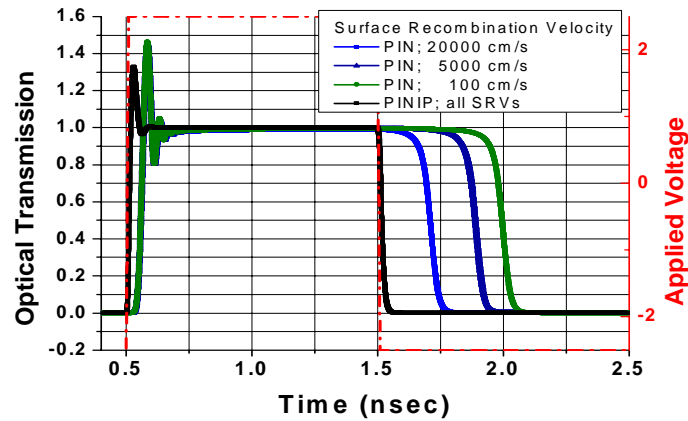


Fig.6: Comparison of transient behavior of PIN and PINIP devices for varying surface conditions as modeled by Surface Recombination Velocity (SRV)

7. High bit rate operation

We have simulated the structure and showed electro-optic modulation at 40 Gbit/s in an NRZ scheme with a resonator of quality factor 5,000. A relatively low quality factor resonator is used since in the absence of electrical fall time limitations, the speed of modulation is now given only by the cavity ring-down time. The proposed device extends the speed of carrier injection modulators from a few Gb/s [24] to as high as 40 Gb/s. Figure 7 shows the applied voltage and corresponding optical transmission profile for an arbitrary bit sequence modulated with an extinction ratio (defined as $10 \log_{10}(P_{\text{high}}/P_{\text{low}})$) of 12 dB at 40 Gbit/s. We assumed a loss of 8 dB/cm in the ring under critical coupling conditions. The insertion loss is 3 dB at 40 Gbit/s with a peak injection of $5 \times 10^{16} \text{ cm}^{-3}$. The insertion loss and extinction ratio can be improved by optimizing the doping profiles [25] or by designing the filter shape using multiple rings [26, 27] or a single add-drop ring filter [28].

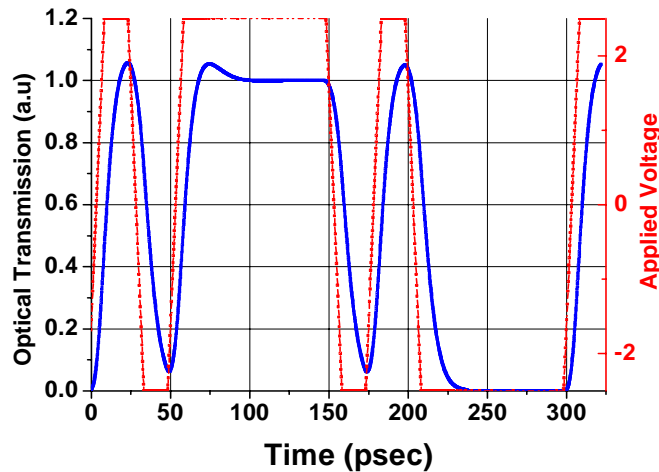


Fig. 7. Optical output for a Non-Return to Zero coded bit stream at 40 Gbit/s.

The maximum sequence of ones (logic high bits) that the device can modulate is $\gg 1000$ bits. The length of identical bit sequence is limited only by the storage time of carriers determined by the leakage current of the device [23] making this an ideal component for on-chip modulation for intra chip communication. The estimated power dissipation of the device is 2.25 fJ/bit/micron length. The energy per bit is estimated from the total charge injected per bit per micron length of the waveguide (0.9 fC/bit/micron) multiplied by the switching voltage (5 V) and the bit transition probability (0.5). The modulator does not draw current while the state is being held except for the parasitic leakage current. This is in contrast to PIN devices where the recombination of carriers has to be compensated with a steady state current inversely proportional to the carrier lifetime. The compact size also avoids the need for traveling wave electrodes and reduces the drive current requirements. The modulator can be driven by an analog CMOS driving circuit made on the same SOI substrate [29].

8. Conclusion

In conclusion, we propose a high speed silicon electro-optic device to increase the modulation rate beyond 40 Gbit/s limited only by the photon lifetime of the cavity. The device shows electrical transitions of 10 ps which is close to the fundamental limit imposed by carrier saturation velocity in silicon for the dimensions dictated by the index contrast in an SOI system. We show 40 Gbit/s operation with a 12 dB extinction ratio and 2.25 fJ/micron energy dissipated per bit in a 10 micron-sized device limited only by the photon lifetime of the structure.

Acknowledgments

This work is sponsored by the Defense Advanced Research Projects Agency supervised by Dr. Jagdeep Shah. The program is executed by the ARO under Contract No. W911NF-06-1-0057 managed by Dr. Wayne Chang. This work is also supported by the National Science Foundation (NSF) under Contract ECS-0300387 and CAREER Grant 0446571;